Profound but Dysfunctional Lymphangiogenesis via Vascular Endothelial Growth Factor Ligands from CD11b$^+$ Macrophages in Advanced Ovarian Cancer

Bong-Hyun Jeon,[1] Cholsoon Jang,[1] Jinah Han,[1] Raghu P. Kataru,[1] Lianhua Piao,[1] Keehoon Jung,[1] Hye Ji Cha,[1] Reto A. Schwendener,[2] Kyu Yun Jang,[3] Kwan-Sik Kim,[3] Kari Alitalo,[4] and Gou Young Koh[1]

[1]National Research Laboratory of Vascular Biology and Biomedical Research Center, Department of Biological Sciences, Korea Advanced Institute of Science and Technology, Daejeon, Republic of Korea; [2]Laboratory of Liposome Research, Institute of Molecular Cancer Research, University of Zurich, Zurich, Switzerland; [3]Department of Pathology and Obstetrics and Gynecology, Chonbuk University Medical School, Jeonju, Republic of Korea; and [4]The Molecular/Cancer Biology Laboratory, Biomedicum Helsinki, University of Helsinki, Helsinki, Finland

Abstract

Severe ascites is a hallmark of advanced ovarian cancer (OVCA), yet the underlying mechanism that creates an imbalance between peritoneal vascular leakage and lymphatic drainage is unknown. Here, we identified and characterized peritoneal lymphatic vessels in OVCA mice, a model generated by implantation of human OVCA cells into athymic nude mice. The OVCA mice displayed substantial lymphangiogenesis and lymphatic remodeling, massive infiltration of CD11b$^+$/LYVE-1$^+$ macrophages and disseminated carcinomatosis in the mesentery and diaphragm, and progressive chylous ascites formation. Functional assays indicated that the abnormally abundant lymphatic vessels in the diaphragm were not conductive in peritoneal fluid drainage. Moreover, lipid absorbed from the gut leaked out from the aberrant mesenteric lymphatic vessels. Our results indicate that vascular endothelial growth factor (VEGF)-C, VEGF-D, and VEGF-A from CD11b$^+$ macrophages are responsible for producing OVCA-induced dysfunctional lymphangiogenesis, although other cell types contribute to the increased ascites formation. Accordingly, the combined blockade of VEGF-C/D and VEGF-A signaling with soluble VEGF receptor-3 and VEGF-Trap, respectively, markedly inhibited chylous ascites formation. These findings provide additional therapeutic targets to ameliorate chylous ascites formation in patients with advanced OVCA. [Cancer Res 2008;68(4):1100–9]

Introduction

Ovarian cancer (OVCA) accounts for 3% to 4% of all cancers in women and is the leading cause of death from gynecologic malignancies (1, 2). Because early-stage OVCA is generally asymptomatic, ~75% of women who develop OVCA are diagnosed at an advanced stage of the disease (1, 2). Patients with advanced OVCA most often present symptoms related to ascites and omental and bowel involvement, including abdominal distension or bloating (2, 3), and rarely present chylous ascites rich in white milky chylomicrons (4, 5). Massive ascites formation is a major cause of morbidity and mortality in patients with OVCA (2). A series of reports (6–8) indicate that vascular endothelial growth factor (VEGF)-A is the primary molecule responsible for producing ascites in OVCA by inducing vascular permeability very strongly in peritoneal microvessels. Consistent with this, blockade of VEGF-A efficiently reduces ascites formation in OVCA animal models (9–11) and also shows promising results in patients with advanced OVCA (12). In addition, previous findings suggest that OVCA-induced ascites may be caused by delayed diaphragmatic lymphatic drainage of peritoneal fluid due to the presence of disseminated OVCA cells that obstruct the draining lymphatic vessels (13). However, how OVCA relates to peritoneal lymphatic vessels is unknown.

Similar to blood vessels, lymphatic vessels possess unique and characteristic morphologic heterogeneity in different tissues and organs (14, 15). Lymphatic vessels play an essential role in the maintenance of tissue fluid homeostasis through regulated uptake of protein-rich interstitial fluid into draining lymphatic vessels and transport of the drained lymphatic fluid into the blood vasculature via collecting lymphatic vessels (16, 17). Lymphatic vessels in the diaphragm provide the main route for draining peritoneal fluid. Lymphatic vessels on the peritoneal side of the diaphragm are attenuated with extremely flattened lumina, whereas lymphatic vessels on the pleural side are tubular, like other lymphatic vessels (18–20). Therefore, the peritoneal fluid absorbed by lymphatic vessels is directly transported into the lymphatic vessels on the pleural side. In contrast, there are very few lymphatic vessels in the central tendon region of the diaphragm. The other sets of lymphatic vessels in intestinal villi and mesentery serve as essential conduits for the absorption and transport of lipids and fluid from the intestine to the thoracic duct and into the blood circulation (16, 17). However, we do not yet know how OVCA affects lymphatic vessels in the diaphragm and mesentery structurally or functionally.

The understanding of the molecular and cellular regulation of new lymphatic vessel formation, "lymphangiogenesis," has greatly advanced in recent years with the recognition of the lymphangiogenic growth factors VEGF-C and VEGF-D (VEGF-C/D) and their lymphatic vessel–specific receptor VEGF receptor-3 (VEGFR-3; reviewed in refs. 21–25). Moreover, proinflammatory cytokine-induced activation of macrophages may be involved in pathologic lymphangiogenesis by reciprocal interactions with the VEGF-C/D-VEGFR-3 system (26–30). Interestingly, primary cells and cell lines derived from OVCA strongly express proinflammatory cytokines,

Note: Supplementary data for this article are available at Cancer Research Online (http://cancerres.aacrjournals.org/).

Requests for reprints: Gou Young Koh, Biomedical Research Center, Department of Biological Sciences, Korea Advanced Institute of Science and Technology, 373-1, Guseong-dong, Daejeon, 305-701, Republic of Korea. Phone: 82-42-869-2638; Fax: 82-42-869-2610; E-mail: gykoh@kaist.ac.kr.

doi:10.1158/0008-5472.CAN-07-2572

including interleukin (IL)-6 and tumor necrosis factor-α (TNF-α; refs. 31, 32), which are known to act as additional factors that promote ascites formation. These proinflammatory cytokines might be involved in pathologic lymphangiogenesis. Therefore, understanding the complex interactions between the VEGF/VEGFR system, macrophages, and possible lymphangiogenesis in OVCA should shed light on the mechanisms associated with severe ascites formation in OVCA.

In this study, we find that OVCA induces strong lymphangiogenesis in the mesenteric and diaphragmatic peritoneum through active proliferation of lymphatic endothelial cells (LEC). Interestingly, the lymphatic vessels formed by the OVCA-induced lymphangiogenesis were nonfunctional in drainage of peritoneal fluid and leaky in drainage of mesenteric chyle. We have defined the underlying mechanisms and the responsible molecules by analysis of critical effector cells and molecules and by using several specific blocking agents. Our results provide a rational basis for future therapies to control chylous ascites formation in patients with OVCA.

Materials and Methods

Animals, culture, and implantation of OVCA cell lines. Specific pathogen-free BALB/cByJ athymic nude (CbyJ.Cg-*Foxn1*^{nu}/J) mice were purchased from The Jackson Laboratory and bred in our pathogen-free animal facility. Animal care and experimental procedures were performed under approval from the Animal Care Committees of Korea Advanced Institute of Science and Technology. The human OVCA lines MDAH-2774, SKOV-3, and OVCAR3 and other cancer cell lines MCF-7, HepG2, U2O2, and HeLa were obtained from the American Type Culture Collection. The cell lines were cultured in DMEM (Life Technologies) containing 10% heat-inactivated fetal bovine serum (HyClone), penicillin, and streptomycin (Sigma-Aldrich) in plastic tissue culture dishes (Nunc) at 37°C in a humidified atmosphere of 5% CO_2. A suspension of the OVCA cells (3×10^7 in 500 μL PBS) was injected into the peritoneal cavity of 8- to 9-week-old female nude mice.

Histologic and morphometric analysis. Abdominal organs, including mesenteries and diaphragms, of the mice were fixed, whole mounted, or embedded with tissue freezing medium (Leica). The tissues were incubated with the blocking solution, one or more of the primary and secondary antibodies. 3,3′-Diaminobenzidine (DAB) and fluorescent signals were visualized, and digital images were obtained using a Zeiss inverted microscope, a Zeiss ApoTome microscope, or a Zeiss LSM 510 confocal microscope. Morphometric measurements of lymphatic vessels in mesentery and diaphragm were made on whole mounts with lymph vessel endothelial hyaluronan receptor-1 (LYVE-1) and Prox-1 immunostaining using photographic analysis in ImageJ software[5] or using a Zeiss ApoTome microscope coupled to a monochrome charge-coupled device camera and image analysis software (AxioVision, Zeiss).

Reverse transcription-PCR and ELISA analyses of VEGF ligands. Each cDNA was made with Reverse Transcription System (Promega), and semiquantitative PCR was performed with the appropriate primers (Supplementary Table S1) with 30 cycles used for the PCR. Quantikine ELISA kits (R&D Systems) were used for measurements of VEGF ligands.

Administration of blocking or depletion agents. To block VEGF-A, mice were given a s.c. injection of VEGF-Trap (25 mg/kg every 3 days s.c. from day 10 after the MDAH-2774 implantation) for the indicated days as previously described (33). To block VEGF-C and VEGF-D, mice were treated with a single i.v. injection of 1×10^9 plaque-forming units (pfu) AdsVEGFR-3 on day 1 after the MDAH-2774 implantation as previously described (34). For systemic depletion of LYVE-1$^+$ and CD11b$^+$ macrophages, mice were treated with i.p. injections of clodronate liposome (CDL; 25 mg/kg every 3 days i.p.) as previously described (35, 36).

Functional assays for lymphatic drainage and intactness. At the indicated days after cell implantation, mice were anesthetized, ascites fluid was aspirated, and the remaining ascites fluid was removed by three flushes with 2 mL PBS. Then, 0.3 mL of India ink was injected into the peritoneal cavity, and the mice were kept on a warm pad in a supine position. To simultaneously visualize India ink staining and LYVE-1$^+$ lymphatic vessels in the diaphragm, 20 min after adding India ink, diaphragms were harvested, fixed with 1% paraformaldehyde in PBS, photographed, immunostained with anti-LYVE-1 antibody and the corresponding horseradish peroxidase–conjugated secondary antibody, processed with DAB, and photographed again. To determine a functional rate of lymphatic drainage of peritoneal fluid into cranial mediastinal lymph node (CMLN) through diaphragmatic lymphatic vessels, 0.5 mL of FITC-dextran (2,000 kDa, 20 mg/mL) was injected into the peritoneal cavity, and the mice were kept on a warm pad in a supine position for the indicated times. The anterior portion of the chest wall was opened, and CMLNs were harvested and homogenized. The fluorescence intensity was detected using a Perkin-Elmer multiplate reader at 510 nm (Wallac Victor^{2}V, Perkin-Elmer). Alternatively, the fluorescence emitted from the CMLN and the thoracic and abdominal cavities was detected by opening the anterior walls of the abdomen and imaging using IVIS imaging system (Xenogen). To examine the intactness of the lipid-transporting mesenteric lymphatic vessels, the mice were deprived of food for 12 h, and 1.0 mL of 10% DMSO solution containing 0.1 mg of BODIPY fluorescent-conjugated lipid tracer (BODIPY FL C_{16}, Molecular Probes) was infused directly into the stomach using a gavage tube. To measure extent of chylous ascites, the levels of chylomicron cholesterol in the ascites were measured by using the Cholesterol/Cholesteryl Ester Quantitation kit (BioVison).

Statistics. Values are presented as mean ± SD. Significant differences between means were determined by ANOVA followed by the Student-Newman-Keuls test. Statistical significance was set at $P < 0.05$.

Results

Implantation of OVCA cell lines into abdominal cavity induces abundant lymphangiogenesis. To examine whether OVCA affects lymphatic vessels in abdominal organs, 3×10^7 of MDAH-2774, OVCAR3, or SKOV-3 cells were implanted into the peritoneal cavity of 8-week-old nude mice. Of these, the mice implanted with the MDAH-2774 cells displayed the earliest and the most massive ascites formation, more often chylous ascites formation, and the widest disseminated carcinomatosis into the i.p. organs (Supplementary Fig. S1*A–D*) compared with the mice implanted with OVCAR3 or SKOV-3 cells. The whole-mounted abdominal organs were immunostained for LECs by using a specific marker, LYVE-1 (37). The mice implanted with the OVCA cells displayed variable but increased density and branching of lymphatic vessels, with markedly increased infiltration of LYVE-1$^+$ (38) or CD11b$^+$ macrophages in the serosal membranes of the mesentery, diaphragm, and abdominal wall. Because the mice implanted with MDAH-2774 cells exhibited more profound lymphangiogenesis than the mice implanted with OVCAR3 or SKOV-3 cells (Supplementary Fig. S1*E*; data not shown), we focused our further experiments in MDAH-2774 model (hereafter referred to as "OVCA mice").

Association of carcinomatosis with lymphangiogenesis in the diaphragm. Consistent with previous reports (18–20), LYVE-1 immunostaining of normal mice revealed the characteristic distribution of lymphatic vessels on both the peritoneal and pleural sides of the diaphragm (Fig. 1*A*; Supplementary Fig. S2). Concomitant with the gradual increase in the attached cancer mass at both the muscular and central tendon regions of the peritoneal

[5] http://rsb.info.nih.gov/ij

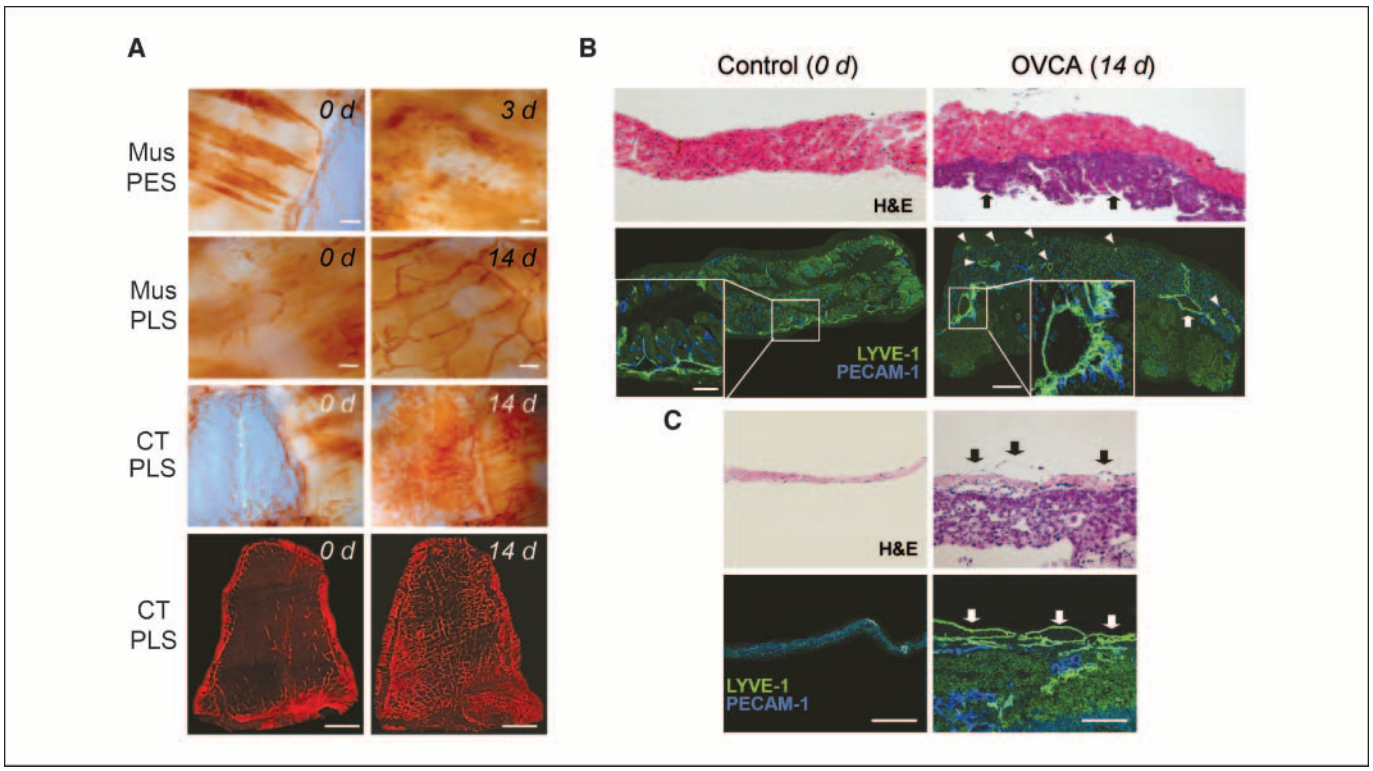

Figure 1. OVCA mice induced lymphangiogenesis in the diaphragm. On the indicated days after the injection of MDAH-2774 cells, diaphragms were harvested and lymphatic vessels were immunostained on the peritoneal side (*PES*) and pleural side (*PLS*) of the diaphragm and are visualized with DAB staining (*brown*). *A,* LYVE-1$^+$ lymphatic vessels in the muscular (*Mus*) and central tendon (*CT*) regions are visualized with DAB (*brown*; *bar*, 200 μm) and fluorescent staining (*red*; *bar*, 1 mm). Muscular (*B*) and central tendon (*C*) regions of diaphragms in control and OVCA mice (14 d) are sagittally sectioned and stained with H&E or immunostained with anti-LYVE-1 (for lymphatic vessels; *green*) and anti-PECAM-1 (for blood vessels; *blue*). Note that the OVCA mice have a massive attached cancer mass (*black arrows*) and irregular spiked and enlarged lymphatic vessels in the peritoneal (*white arrows*) and pleural (*white arrowheads*) side of the muscular region of diaphragm. *Black* and *white arrowheads,* moreover, the OVCA mice have substantial number of enlarged lymphatic vessels in the pleural side of the central tendon. *Bar,* 100 μm.

side of the diaphragm, the OVCA mice displayed increased aberrant lymphatic branching at the muscular region of the pleural side of diaphragm and gradual formation of a gigantic mesh-like lymphatic sheets in central tendon region (Fig. 1*A*). The typical structure of lymphatic strips was disrupted, and several dilated and fragmented lymphatic vessels were observed in the muscular region on the peritoneal side starting at 3 days after the MDAH-2774 implantation (Fig. 1*A*). Irregular and gigantic mesh-like lymphatic sheets were observed in the central tendon region at 14 and 21 days after the MDAH-2774 implantation (Fig. 1*A*). Sagittal sections of muscular region of the diaphragm showed a massive attached tumor mass on the peritoneal side (Fig. 1*B*). The diaphragms displayed enlarged and irregularly spiked lymphatic vessels in the serosal membrane between the cancer mass and the muscle (Fig. 1*B*). In addition, sagittal sections of the central tendon region of the diaphragm showed similar changes, including enlarged lymphatic vessels as "reactive lymphangiogenesis" on the pleural side (Fig. 1*C*).

OVCA mice display profound lymphangiogenesis in the mesentery. Lymphatic density and branching at the mesenteric-intestinal border and mesentery gradually increased over time in the OVCA mice (Fig. 2*A* and *C*). Using double immunostaining for LYVE-1 and Prox-1 (39), we confirmed that these remodeled vessels were lymphatic vessels (Fig. 2*B*). The vessels had many sprouts and filopodia (40) in the mesentery (Fig. 2*B*). The number of LYVE-1$^+$ macrophages (38) increased profoundly within 7 days after MDAH-2774 cell implantation, and no further significant increases but similar densities of LYVE-1$^+$ macrophages were found until 21 days after implantation (Fig. 2*A* and *D*).

Aberrant lymphangiogenesis in OVCA mice occurs mainly through proliferation of LECs. To investigate whether the observed lymphangiogenesis and lymphatic remodeling resulted from proliferation of LECs or by extension and hypertrophy of LECs, we used double immunostaining for LYVE-1/phosphohistone 3 (nuclear protein of dividing cells) and LYVE-1/Prox-1. A greater number of phosphohistone 3$^+$ LECs and increased lymphatic densities were observed in the muscular region (Supplementary Fig. S3*A*) and central tendon region (Supplementary Fig. S3*B* and *D*) of the OVCA mice compared with the control mice. Notably, a gigantic mesh-like lymphatic sheet formed and covered almost all of the central tendon area by 21 days after the MDAH-2774 implantation, and the number of Prox-1$^+$ cells increased in correlation with lymphatic area in this region over time (Supplementary Fig. S3*C, E*, and *F*), indicating that proliferation of LECs is the main event for the OVCA-induced lymphangiogenesis. Furthermore, the lymphatic vessels displayed abundant sprouts and filopodia at 14 days after implantation, whereas those of the control mice displayed round and smooth initial lymphatic vessels (Supplementary Fig. S4*A*).

LYVE-1$^+$ and CD11b$^+$ macrophages associate with the growing lymphatic vessels. We further characterized the LYVE-1$^+$ macrophages in the OVCA mice because macrophage activation is involved in lymphangiogenesis (26–30). Fluorescence-activated cell sorting (FACS) analysis of the macrophages of mesentery in the

OVCA mice revealed two subpopulations of CD11b$^+$ macrophages (Fig. 3*A*): CD11b$^+$/LYVE-1$^+$ (~73.6%) and CD11b$^+$/LYVE-1$^-$ (~17.8%; n = 8 of 14-d OVCA mice). Higher magnifications revealed that CD11b$^+$ low/LYVE-1$^+$ macrophages were closely located with growing LYVE-1$^+$ lymphatic vessels, frequently with bidirectional filopodia formation (Fig. 3*B* and *C*; Supplementary Fig. S4*B*). In addition, triple immunostaining in the junctional areas of the muscle and central tendon regions of the diaphragm revealed that the growing lymphatic vessels expressed not only VEGFR-3 but also VEGFR-2, whereas the quiescent lymphatic vessels did not express VEGFR-2. The growing blood vessels were negative for VEGFR-3 (Fig. 3*D*), which is different from other tumor models (41, 42) and from developing blood vessels in embryo (43), which are positive for VEGFR-3. Thus, LYVE-1$^+$ and CD11b$^+$ macrophages and up-regulation of lymphatic endothelial VEGFR-2 were closely associated with the growing lymphatic vessels in the OVCA mice.

Host CD11b$^+$ macrophages and OVCA cells as sources of lymphangiogenic VEGF ligands. To investigate the source of the expression and secretion of lymphangiogenic factors that drive the OVCA-induced lymphangiogenesis, a series of reverse transcription-PCR (RT-PCR) and ELISA assays were performed using the cultured OVCA cells, host tissues, isolated CD11b$^+$ macrophages, and ascites. Similar to previous reports (31, 32), the OVCA cell lines (MDAH-2774, OVCAR3, and SKOV-3) expressed relatively high levels of VEGF-A_{165}, VEGF-A_{121}, VEGF-C, VEGF-D, and proinflammatory cytokines, including TNF-α, IL-1β, and IL-6, when compared with other carcinoma cell lines, including MCF-7, HepG2, U2O2, and HeLa. At 14 days after implantation of MDAH-2774 cells into the peritoneal cavity, expression of VEGF-C and VEGF-D in the growing OVCA cells increased moderately in the diaphragm and mesentery, whereas no significant changes were observed in VEGF-A expression (Fig. 4*A*). In comparison, expression of host VEGF-A, TNF-α, and IL-1β markedly increased in the host diaphragm and mesentery, whereas expression of host VEGF-C, VEGF-D, and IL-6 increased slightly (Fig. 4*B*). Expression of host VEGF ligands in isolated CD11b$^+$ cells from the OVCA mice was markedly higher [VEGF-A_{164} (~14-fold), VEGF-C (~39-fold), and VEGF-D (~121-fold)] than that seen in control mice (Fig. 4*C*). ELISA revealed that the amounts of VEGF-A and VEGF-C derived from the OVCA cells in the ascites gradually increased, whereas VEGF-D amount increased only

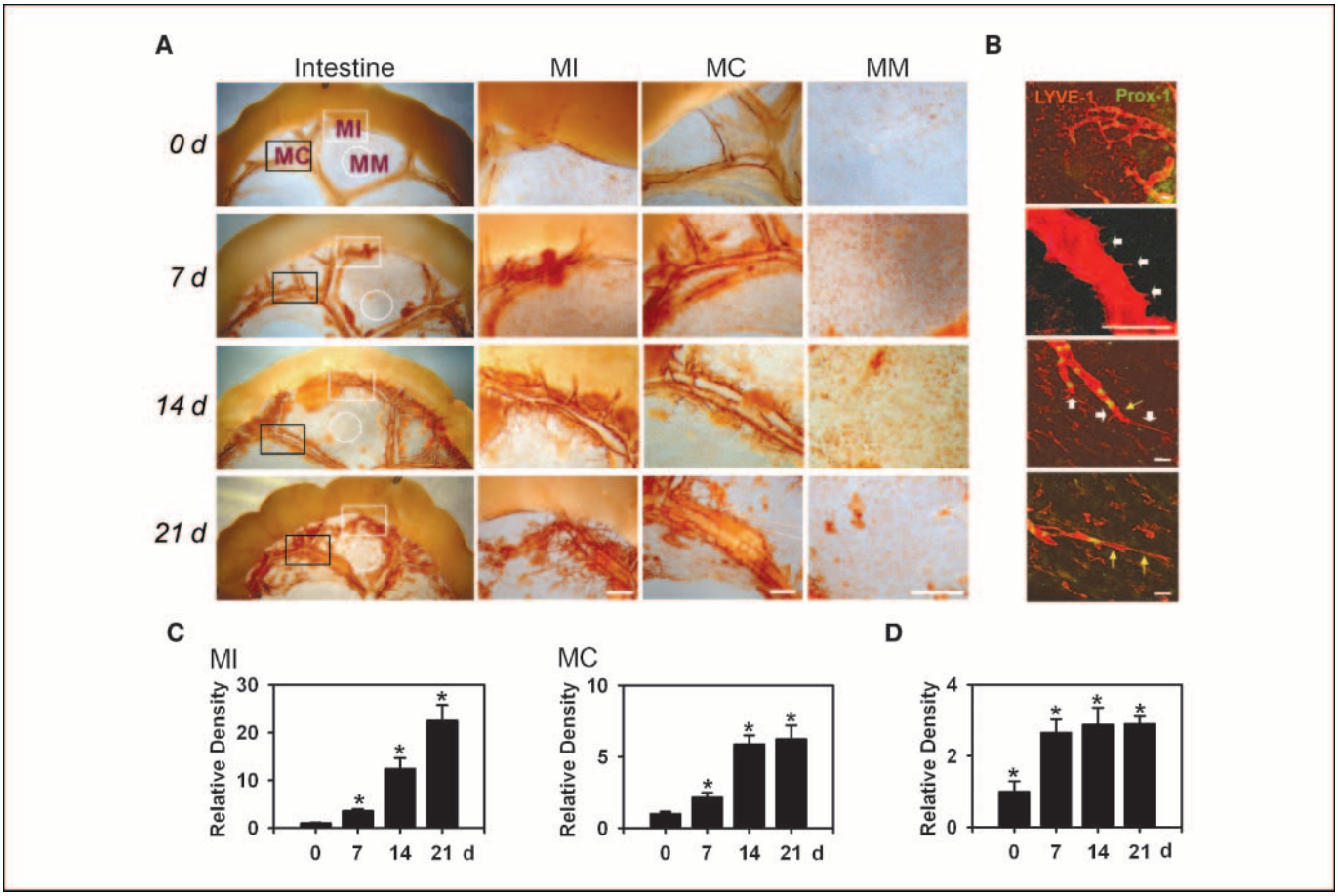

Figure 2. OVCA mice display profound lymphangiogenesis in the mesentery. MDAH-2774 cells (3×10^7) were injected into the peritoneal cavity of 8- to 9-week-old female nude mice. *A,* on the indicated days, ileum was harvested and immunostained with anti-LYVE-1 antibody. LYVE-1$^+$ lymphatic vessels at the mesenteric-intestinal border (*MI*; *white square line*), mesenteric-collecting lymphatic vessels (*MC*; *black square line*), and LYVE-1$^+$ macrophages in the mesenteric membrane (*MM*; *white circle line*) are visualized with DAB staining (*brown*). *Bar,* 400 μm. *B,* at 14 d, LYVE-1$^+$/Prox-1$^+$ lymphatic vessels are distinguished from LYVE-1$^+$ macrophages in the mesentery. LYVE-1$^+$ lymphatic vessels have abundant branching, sprouting (*yellow arrows*), and filopodia (*white arrows*). *Bar,* 25 μm. LYVE-1$^+$ lymphatic densities in the mesenteric-intestinal border and mesenteric-collecting lymphatic vessels (*C*) and LYVE-1$^+$ macrophage densities in the mesenteric membrane (*D*) in a given area were quantified and represented as fold with 0 d arbitrarily given as 1. *Columns,* mean of four to five mice; *bars,* SD. *, $P < 0.05$ versus 0 d.

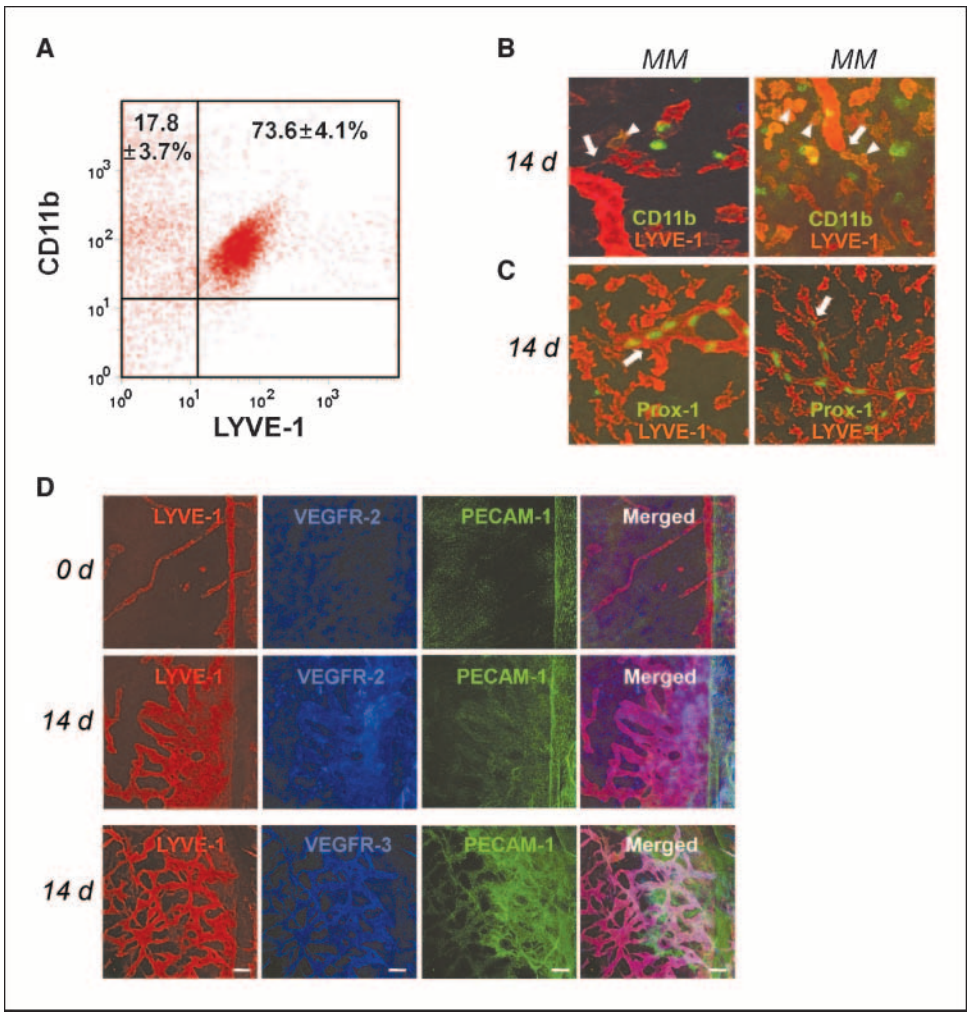

Figure 3. LYVE-1$^+$ and CD11b$^+$ macrophages, VEGFR-2, and VEGFR-3 are closely associated with the growing lymphatic vessels of OVCA mice. At 14 d after tumor inoculation, mesenteries and diaphragms are harvested. *A,* CD11b$^+$ cells are enriched from mesenteries and analyzed by FACS for LYVE-1$^+$ cells. Numbers are mean ± SD from four mice. *B* and *C,* double immunostainings for LYVE-1 (*red*) and CD11b (*green*) or Prox-1 (*green*) are performed in the mesenteric membrane. *Arrows,* filopodia or close junctional areas between LECs and macrophages; *arrowheads,* yellowish green CD11b$^+$/LYVE-1$^+$ macrophages. *Bar,* 100 μm. *D,* triple immunostaining for LYVE-1 (*red*), VEGFR-2 or VEGFR-3 (*blue*), and PECAM-1 (*green*) in the muscular central tendon junction region. *Bar,* 100 μm.

slightly (Fig. 4*D*). In comparison, the amount of host VEGF-A in the ascites markedly increased at days 14 and 21 (Fig. 4*D*), being approximately 6.9- and 8.1-fold higher than the amount of OVCA cell–derived VEGF-A at days 14 and 21. Thus, host CD11b$^+$ macrophages and OVCA cells are the main sources of i.p. lymphangiogenic VEGF ligands in the OVCA mice.

OVCA-induced lymphatic vessels are dysfunctional and display impaired peritoneal fluid drainage. To assess the drainage function of the diaphragmatic lymphatic vessels, we injected India ink i.p. (300 μL; ref. 20). At 20 min after the injection, most lymphatic vessels of the muscular region on both sides of the diaphragm in the control mice contained ink, whereas almost no lymphatic vessels of the central tendon area contained ink (Fig. 5*A–D*; Supplementary Fig. S5). In contrast, lymphatic vessels containing India ink were not observed on the peritoneal side of diaphragm of the OVCA mice because of the attached OVCA mass (Supplementary Fig. S6). Only large lymphatic vessels that had taken up ink were seen on the pleural side of the diaphragm (Fig. 5*A* and *B*). Interestingly, most of the gigantic mesh-like lymphatic sheet in the central tendon region having the OVCA mass did not contain ink (Fig. 5*A* and *B*), which was instead mainly located on the pleural side in this region. Thus, the gigantic mesh-like lymphatic vessels were nonfunctional in draining peritoneal fluid from the abdominal cavity. However, there was a scattered and moderate amount of ink in the areas of lacking lymphatic vessels (Fig. 5*A*), suggesting that there had been transfer of peritoneal fluid by aberrant leakage. These observations led us to estimate peritoneal fluid drainage to the lymph nodes between control and OVCA mice.

Lymphatic fluid collected in the diaphragm drains into the right lymphatic duct via the CMLN and tracheal lymphatic trunk (44, 45). As the second pathway, it is transported to the thoracic duct via the caudal mediastinal lymph node (44, 45). Because the CMLN is relatively accessible and visible by simple microsurgery, we analyzed the drainage rate by detection of FITC-dextran (molecular weight, 2,000 kDa) in the CMLN at 20 min after its i.p. injection. The drainage in the OVCA mice was significantly slower than that of the control mice at various time points (Fig. 5*C*). Moreover, on feeding the mice with the BODIPY fluorescent-conjugated lipid tracer, the absorbed lipid tracer absorbed from the gut leaked from the aberrant mesenteric lymphatic vessels in the OVCA mice, whereas it was transported in the mesenteric lymphatic vessels without leakage in the control mice (Fig. 5*D*). Thus, the leaky misrouted mesenteric lymphatic vessels could contribute to the formation of chylous ascites in the OVCA mice.

Inhibition of OVCA-associated lymphangiogenesis by blocking VEGF/VEGFR or depletion of macrophages. We next examined the role of the VEGF signals and the macrophages in

the OVCA-induced dysfunctional lymphangiogenesis by using specific blocking and depletion agents. To block VEGF-A, VEGF-Trap (33) was produced using the Chinese hamster ovary cell expression system (Supplementary Fig. S7; ref. 46). To block VEGF-C and VEGF-D, an adenovirus encoding the soluble extracellular domain of VEGFR-3 (AdsVEGFR-3) was used (34). Treatment with VEGF-Trap or AdsVEGFR-3 significantly reduced the density, branching, and sprouting of the aberrant lymphatic vessels not only in the mesentery but also in the diaphragm without a significant reduction of tumor volume (Fig. 6*A* and *B*). As controls, dimeric Fc protein or 1×10^9 pfu AdLacZ was injected in the same manner. The mice treated with the dimeric Fc protein or the AdLacZ showed no difference from the mice treated with control buffer, PBS. To deplete macrophages, i.p. treatment with CDL (25 mg/kg every 3 days i.p. from day 0 after the MDAH-2774 implantation) was performed (35, 36). As a control, empty liposome was injected in the same manner. The CDL treatment efficiently depletes macrophages in all organs of the abdominal cavity by inducing selective apoptosis of macrophages (Supplementary Fig. S8). In this situation, the density, branching, and sprouting of the aberrant lymphatics in the mesentery and diaphragm were markedly reduced without significant reduction of tumor volume (Fig. 6*A* and *B*). In contrast, the mice treated with the control liposome showed no difference from the mice treated with control buffer, PBS. These results indicate that VEGF-A, VEGF-C, VEGF-D, and macrophages are the main mediators of OVCA-induced aberrant lymphangiogenesis.

Notably, VEGF-Trap treatment markedly reduced ascites formation, whereas the treatments with AdsVEGFR-3 and CDL did not affect significantly ascites formation (Fig. 6*C*), indicating that VEGF-A is the main mediator for inducing ascites formation in OVCA. As mentioned previously, the host tissues (diaphragm and mesentery) and $CD11b^+$ macrophages in the OVCA mice were the main source of VEGF-A. Of these, VEGF-A secreted from the host tissues could be the main mediator for OVCA-induced ascites formation, whereas VEGF-A secreted from the macrophages could be the main mediator for OVCA-induced lymphangiogenesis. To address this possibility, we measured mouse VEGF-A, mouse IL-6, and human VEGF-A in the peritoneal fluid of the OVCA mice treated with CDL or control liposome. There were no differences in mouse IL-6 between the mice treated with CDL and the mice treated with control liposome, whereas mouse VEGF-A and human VEGF-A levels were slightly, but not significantly, lower in the mice treated with CDL than the mice treated with control liposome (Supplementary Table S2). These data indicate that VEGF-A secreted from the host tissues, not from the infiltrating macrophages, could be main mediator for OVCA-induced ascites formation. As the result of chylous leak from mesenteric lymphatic vessels, amounts of chylomicron cholesterol in the ascitic fluid of the OVCA mice were ~560 μg (Fig. 6*D*), whereas those in the

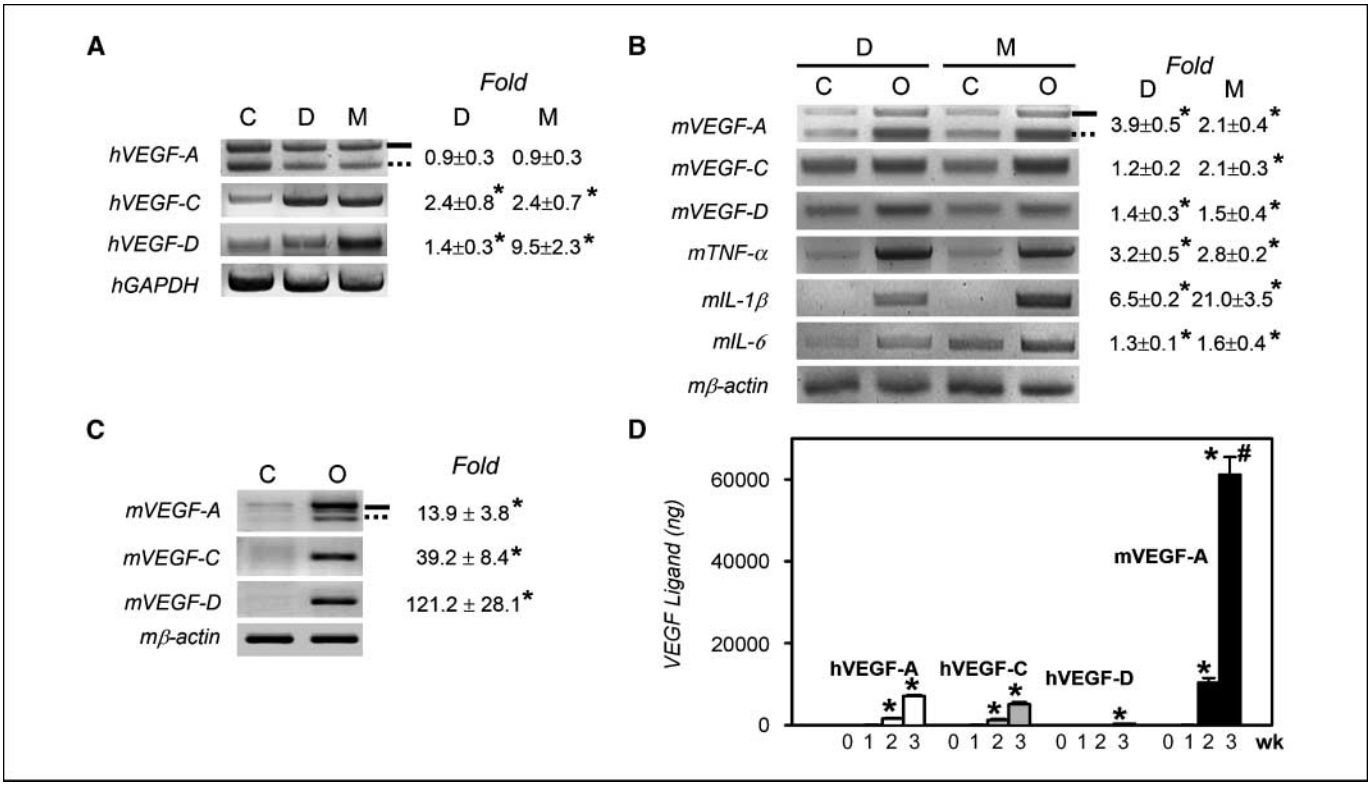

Figure 4. Paracrine lymphangiogenic role of $CD11b^+$ macrophages and growing OVCA cells. *A,* RT-PCR comparisons of human VEGF (*hVEGF*) ligands in cultured MADH-2274 cells (*C*) and in growing MDAH-2274 cells from the diaphragm (*D*) and mesentery (*M*) of the 14-d OVCA mice. *B,* RT-PCR comparisons of mouse VEGF (*mVEGF*) ligands and proinflammatory cytokines in the diaphragm and mesentery in the control (*C*) and the 14-d OVCA (*O*) mice. *C,* RT-PCR comparisons of mouse VEGF ligands in enriched $CD11b^+$ macrophages from i.p. cavities between the control and the 14-d OVCA mice. *Fold,* the densitometric analyses are presented as the relative fold after normalization with human glyceraldehyde-3-phosphate dehydrogenase (*hGAPDH*) or mouse β-actin (*mβ-actin*) or mouse GAPDH; control is arbitrarily regarded as 1. Numbers represent the mean ± SD from three experiments. *, $P < 0.05$ versus control. *Solid bar,* human $VEGF\text{-}A_{165}$ or mouse $VEGF\text{-}A_{164}$; *dotted bar,* human $VEGF\text{-}A_{121}$ or mouse $VEGF\text{-}A_{120}$. *D,* ELISA comparisons of i.p. amounts of VEGF ligands in the OVCA mice at the indicated weeks. *Columns,* mean of three to four mice; *bars,* SD. *, $P < 0.05$ versus 0 wk; #, $P < 0.05$ versus hVEGF-A of 3 wk.

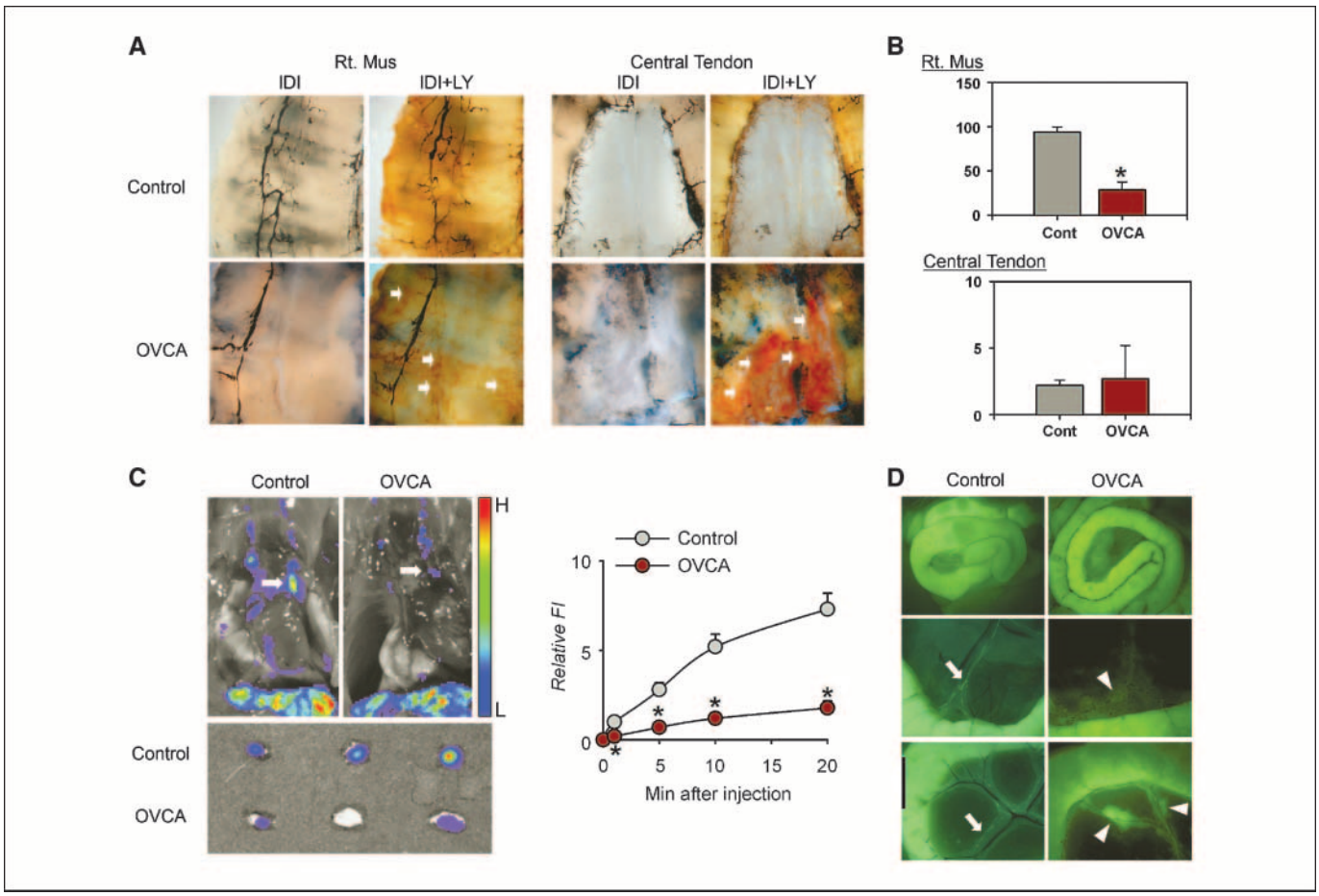

Figure 5. OVCA-induced aberrant lymphatic vessels in the diaphragm are dysfunctional and display defective peritoneal fluid drainage. *A,* the control and OVCA mice (21 d) were treated with an i.p. injection of India ink. At 20 min after injection, the pleural side of the diaphragms was photographed, fixed, and immunostained with anti-LYVE-1 antibody (*IDI+LY*). *Rt. Mus,* right side of muscular region. *White arrows,* LYVE-1$^+$/India ink–negative nonfunctional lymphatic vessels. *B,* the ink contained within functional lymphatic vessels in the right side of muscular region of the pleural side and central tendon region of diaphragms was quantified as the density of ink-containing lymphatics per LYVE-1$^+$ lymphatics and represented as a percentage. *Columns,* mean of four mice; *bars,* SD. *, $P < 0.05$ versus control mice (*Cont*). *C, left,* the control and OVCA mice (14 d) were treated with an i.p. injection of 300 μL of FITC-dextran. At 20 min after injection, the anterior wall of the chest was opened and the fluorescence intensity in the chest areas was measured, including the CMLN (*top, white arrows*) and the dissected CMLN (*bottom, left*). The color scale indicates fluorescence intensity (*FI*; photons/s/cm^2/steradian). *Top red,* maximum fluorescence intensity (*H*); *bottom blue,* minimum fluorescence intensity (*L*). *Right,* at the indicated times later, CMLNs were dissected and the fluorescence intensity was measured. Fluorescence is quantified and represented as fold, with the intensity of CMLN at 1 min in the control mouse arbitrarily given as 1. *Points,* mean of four mice; *bars,* SD. *, $P < 0.05$ versus control. *D,* BODIPY fluorescent-conjugated lipid tracer was infused into the stomachs of the control and OVCA mice. Two hours later, intestines and mesenteric lymphatic vessels were photographed with a dissecting fluorescence microscope. *Arrows,* normally transporting lipids; *arrowheads,* leaky lipids. The results from four experiments were similar.

peritoneal fluid of normal mice were <1.0 μg. Intriguingly, in the OVCA mice, treatment of AdsVEGFR-3 or CDL resulted in reduction of the amount of chylomicron cholesterol of approximately 66% or 62%, and treatment of VEGF-Trap resulted in reduction of the amount of chylomicron cholesterol of ~38% (Fig. 6*D*). Importantly, simultaneous treatment of VEGF-Trap and AdsVEGFR-3 resulted in marked reduction of the amount of chylomicron cholesterol of up to ~82% in the OVCA mice (Fig. 6*D*). Thus, combined blockade of VEGF-A and VEGF-C/D effectively suppressed chylous ascites formation.

Discussion

Here, we report that the mouse OVCA model displays abundant dysfunctional and leaky lymphangiogenesis in the mesentery and diaphragm via VEGF ligands secreted by tumor-associated CD11b$^+$ macrophages. Our data also explain why late-stage OVCA induces chylous ascites formation despite increased lymphangiogenesis in the diaphragm and mesentery. Our analysis indicated that the OVCA-induced lymphangiogenesis mainly occurs via proliferation of LECs, coupled with intense vessel remodeling as shown by copious branching, sprouting, and filopodia. Notably, LYVE-1$^+$ and CD11b$^+$ macrophages massively infiltrated the areas where lymphangiogenesis and lymphatic remodeling occurred (Supplementary Fig. S9*A*). Thus, OVCA-induced lymphangiogenesis and lymphatic remodeling is much more extensive than solid tumor–induced lymphangiogenesis and lymphatic remodeling comprising variable extents of lymphatic vessel growth in the tumor periphery (peritumoral) and to a lesser degree within the tumors (22, 23, 25, 47).

Our blocking experiments with VEGF-Trap and sVEGFR-3 indicated that VEGF-A, VEGF-C, and VEGF-D play major roles in the observed lymphangiogenesis and lymphatic remodeling (Fig. 6*A*). In fact, VEGFR-3 and VEGFR-2 have overlapping contributions in lymphangiogenesis (48). For example, proteolytically processed VEGF-C and VEGF-D activate VEGFR-2, although

their capacity to activate this receptor is lower than that of VEGF-A (49, 50). Furthermore, LECs express low levels of VEGFR-2 that are enhanced during embryonic development, wound healing, and tumor progression. Thus, lymphangiogenesis is not entirely dependent on VEGFR-3 in certain conditions (21, 25). Indeed, our coimmunostaining analyses revealed that, in OVCA-induced lymphangiogenesis, the LECs strongly expressed both VEGFR-2 and VEGFR-3 (Fig. 6*A*). Therefore, all three VEGF ligands could be major mediators of OVCA-induced profound lymphangiogenesis. In comparison, the bronchial epithelial cells expressed mainly VEGFR-2 in OVCA-induced angiogenesis, which is different from other solid tumors and developing blood vessels that express both VEGFR-2 and VEGFR-3 (41–43). Therefore, among the three VEGF ligands, only VEGF-A could be a major mediator of OVCA-induced angiogenesis.

Macrophages were also significant in lymphangiogenesis in the OVCA mice. As confirmed by the RT-PCR, the OVCA cells secrete many proinflammatory cytokines (31, 32), which stimulate macrophage recruitment and infiltration (Supplementary Fig. S9*A*). Our RT-PCR and ELISA analyses indicate that the host $CD11b^+$ macrophages are a major source of VEGF ligands for the OVCA-induced lymphangiogenesis. To a lesser extent, the OVCA cells provide a source of VEGF ligands. Accordingly, the depletion of macrophages by CDL in the OVCA mice markedly reduced OVCA-induced lymphangiogenesis (Supplementary Fig. S9*A*). Moreover, most $CD11b^+/LYVE\text{-}1^+$ macrophages were closely located in the growing lymphatic vessels. LYVE-1/Prox-1 coimmunostaining revealed a close interaction between these cells and the LECs of remodeling lymphatic vessels via endothelial filopodia (40). However, we have no evidence that the macrophages are incorporated or transdifferentiated into LECs of growing and remodeling lymphatic vessels in the OVCA mice. Rather, they would secrete lymphangiogenic factors in a paracrine manner.

Consistent with previous reports (6–13), VEGF-A was highly abundant and induced ascites formation in the OVCA mice, as evidenced by the ability of the VEGF-Trap to reduce the ascites formation. In contrast, sVEGFR-3 and CDL did not significantly reduce ascites formation. Given that there was no significant reduction in ascites volume, but there was substantial reduction of aberrant lymphangiogenesis by the blocking of VEGF-C/D or the depletion of macrophages, OVCA-induced ascites formation mainly results from VEGF-A derived from host tissue, but not from

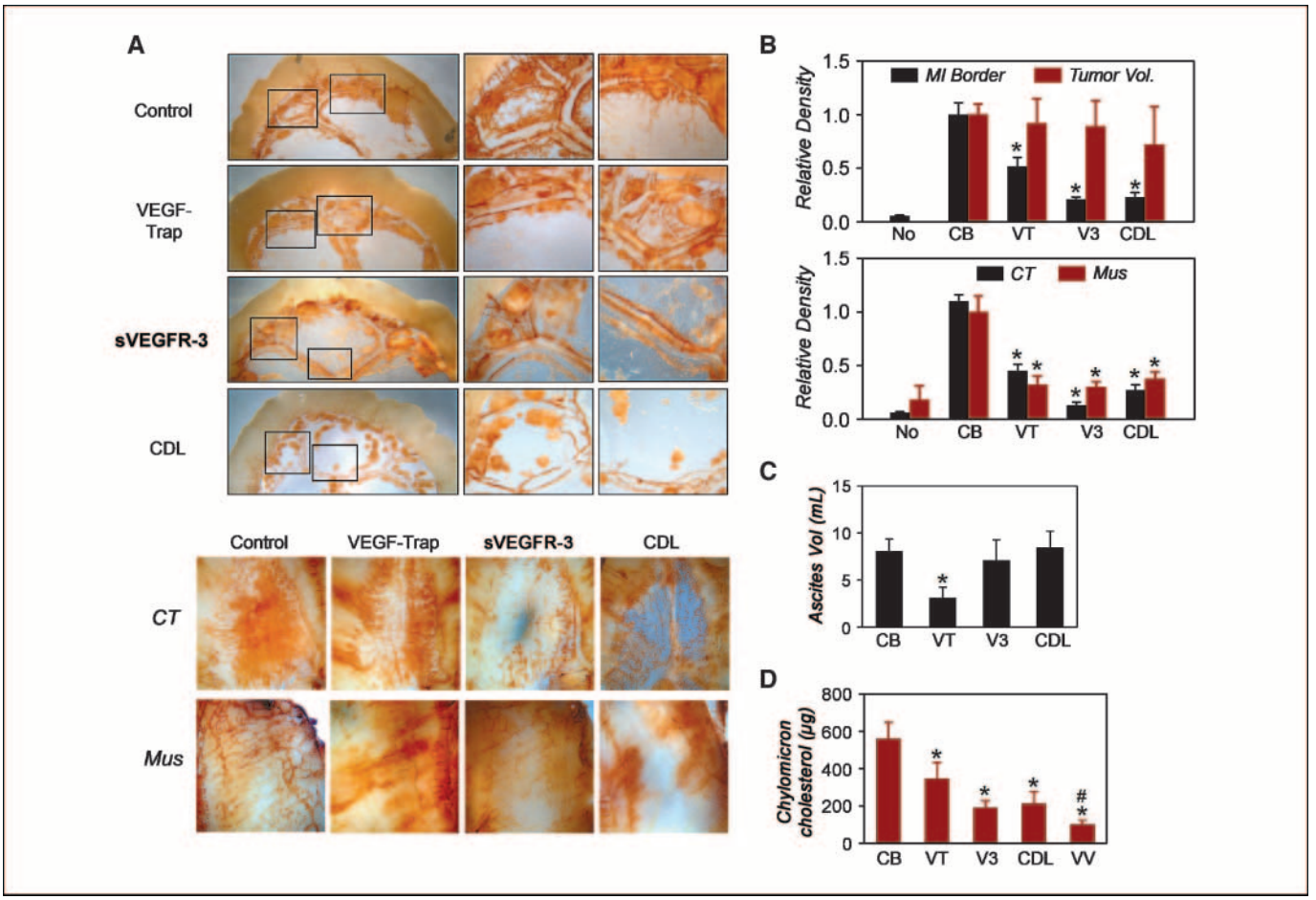

Figure 6. Blockade of VEGF/VEGFR signaling or depletion of macrophages reduces the aberrant lymphangiogenesis. On the day of tumor inoculation, nude mice were treated with CDL. At the appropriate times later, mice were treated with VEGF-Trap (*VT*), sVEGFR-3 (*V3*), or both (*VV*). At 21 d, mesenteries and diaphragms are harvested and immunostained with anti-LYVE-1. *A,* $LYVE\text{-}1^+$ lymphatic vessels in mesenteries (*top four panels*) and central tendon and muscular regions on the pleural side of the diaphragm (*bottom two panels*) are visualized with DAB staining (*brown*). *B,* quantification of mesenteric tumor volumes and of $LYVE\text{-}1^+$ lymphatic densities in mesenteric-intestinal (*MI*) border, central tendon, and muscular regions on the pleural side of the diaphragm. Values are represented as fold, with the value for control buffer (*CB*) arbitrarily given as 1. *C* and *D,* ascites volumes and total amounts of chylomicron cholesterol in ascites were measured. *No,* normal mice. *Columns,* mean of three to five mice; *bars,* SD. *, $P < 0.05$ versus normal mice or control buffer; #, $P < 0.05$ versus VEGF-Trap, sVEGFR-3, or CDL.

VEGF-A derived from the infiltrating macrophages, through enhancing vascular leakage in the abdominal wall, including the peritoneum, possibly in a paracrine manner. Moreover, it should be noted that there was still insufficient functional compensation of diaphragmatic lymphatic vessels to drain excess peritoneal fluid induced by OVCA, although the aberrant lymphangiogenesis was largely reduced by the blocking of VEGF-C/D or the depletion of macrophages. Our functional assays with India ink provide a striking demonstration of the uncoupling of the copious lymphatic vessels of the diaphragm from peritoneal fluid drainage. Consistent with a previous report (20), the lymphatic vessels of both sides of the diaphragm are functionally coupled. However, in the OVCA mouse model, not only was preexisting lymphatic vessel function in the muscular region disrupted but also the new lymphatics formed by OVCA-induced lymphangiogenesis were uncoupled from peritoneal fluid drainage (Supplementary Fig. S9*B* and *C*). Moreover, the mesh-like lymphatic vessels on the pleural side of the central tendon were poorly functional. These dysfunctions of the lymphatic vessels could be caused by the attached OVCA tumor mass on the pleural side of the diaphragm (Supplementary Fig. S9*B* and *C*). Chylous ascites is occasionally observed in patients with OVCA (1–3), but most patients have been diagnosed by physical examination during operation. Our study use of the lipid tracer and measurement of chylomicron cholesterol in the ascitic fluid provided compelling evidence that the chyle from mesenteric lymphatic vessels leaks into the peritoneal cavity of the OVCA mice. Therefore, a high number of patients with advanced OVCA may have "microchylous ascites formation" if one may reevaluate the ascites with more sensitive and accurate methods. Moreover, our blocking experiment with sVEGFR-3 and CDL indicated that VEGF-C and VEGF-D secreted from $CD11b^+$ low/$LYVE\text{-}1^+$ macrophages in mesentery played a key role in generating the leaky lymphatic vessels. Furthermore, it is important to note that the combined blockades of the VEGF-A responsible for ascites formation and the VEGF-C and VEGF-D responsible for chylous leak effectively suppress the chylous ascites formation.

In summary, a profound but dysfunctional and leaky lymphangiogenesis could be one of the hallmarks of advanced OVCA and may contribute to chylous ascites formation. VEGF family ligands secreted from $CD11b^+$ macrophages in the peritoneal cavity are the main stimulating factors for OVCA-induced aberrant lymphangiogenesis. Our study provides additional selective therapeutic targets to inhibit chylous ascites formation in patients with advanced OVCA.

Acknowledgments

Received 7/7/2007; revised 11/26/2007; accepted 12/19/2007.

Grant support: Korea Science and Engineering Foundation through the National Research Laboratory Program 2004-02376 (G.Y. Koh) funded by the Ministry of Science and Technology.

The costs of publication of this article were defrayed in part by the payment of page charges. This article must therefore be hereby marked *advertisement* in accordance with 18 U.S.C. Section 1734 solely to indicate this fact.

References

1. Jemal A, Siegel R, Ward E, Murray T, Xu J, Thun MJ. Cancer statistics 2007. CA Cancer J Clin 2007;57:43–66.
2. Colombo N, Van GT, Parma G, et al. Ovarian cancer. Crit Rev Oncol Hematol 2006;60:159–79.
3. Aalami OO, Allen DB, Organ CH. Chylous ascites: a collective review. Surgery 2000;128:761–78.
4. Boran N, Cil AP, Tulunay G, Ozgul N, Kose MF. Chylous ascites following para-aortic lymphadenectomy: a case report. Gynecol Oncol 2004;93:711–4.
5. Wright JD, Hagemann A, Rader JS, et al. Bevacizumab combination therapy in recurrent, platinum-refractory, epithelial ovarian carcinoma: a retrospective analysis. Cancer 2006;107:83–9.
6. Luo JC, Yamaguchi S, Shinkai A, Shitara K, Shibuya M. Significant expression of vascular endothelial growth factor/vascular permeability factor in mouse ascites tumors. Cancer Res 1998;58:2652–60.
7. Nagy JA, Masse EM, Herzberg KT, et al. Pathogenesis of ascites tumor growth: vascular permeability factor, vascular hyperpermeability, and ascites fluid accumulation. Cancer Res 1995;55:360–8.
8. Nagy JA, Morgan ES, Herzberg KT, Manseau EJ, Dvorak AM, Dvorak HF. Pathogenesis of ascites tumor growth: angiogenesis, vascular remodeling, and stroma formation in the peritoneal lining. Cancer Res 1995;55:376–85.
9. Byrne AT, Ross L, Holash J, et al. Vascular endothelial growth factor-trap decreases tumor burden, inhibits ascites, and causes dramatic vascular remodeling in an ovarian cancer model. Clin Cancer Res 2003;9:5721–8.
10. Hu L, Hofmann J, Holash J, Yancopoulos GD, Sood AK, Jaffe RB. Vascular endothelial growth factor trap combined with paclitaxel strikingly inhibits tumor and ascites, prolonging survival in a human ovarian cancer model. Clin Cancer Res 2005;11:6966–71.
11. Mesiano S, Ferrara N, Jaffe RB. Role of vascular endothelial growth factor in ovarian cancer: inhibition of ascites formation by immunoneutralization. Am J Pathol 1998;153:1249–56.
12. Monk BJ, Han E, Josephs-Cowan CA, Pugmire G, Burger RA. Salvage bevacizumab (rhuMAB VEGF)-based therapy after multiple prior cytotoxic regimens in advanced refractory epithelial ovarian cancer. Gynecol Oncol 2006;102:140–4.
13. Feldman GB, Knapp RC, Order SE, Hellman S. The role of lymphatic obstruction in the formation of ascites in a murine ovarian carcinoma. Cancer Res 1972;32:1663–6.
14. Ji RC. Lymphatic endothelial cells, lymphangiogenesis, and extracellular matrix. Lymphat Res Biol 2006;4:83–100.
15. Pepper MS, Skobe M. Lymphatic endothelium: morphological, molecular and functional properties. J Cell Biol 2003;163:209–13.
16. von Andrian UH, Mempel TR. Homing and cellular traffic in lymph nodes. Nat Rev Immunol 2003;3:867–8.
17. Saladin KS. Anatomy & physiology: the unity of form and function. In: The lymphatic and immune system. Boston (MA): McGraw Hill; 2004. p.799–835.
18. Tsilibary EC, Wissig SL. Light and electron microscope observations of the lymphatic drainage units of the peritoneal cavity of rodents. Am J Anat 1987;180:195–207.
19. Azzali G. The lymphatic vessels and the so-called "lymphatic stomata" of the diaphragm: a morphologic ultrastructural and three-dimensional study. Microvasc Res 1999;57:30–43.
20. Shinohara H. Lymphatic system of the mouse diaphragm: morphology and function of the lymphatic sieve. Anat Rec 1997;249:6–15.
21. Hong YK, Shin JW, Detmar M. Development of the lymphatic vascular system: a mystery unravels. Dev Dyn 2004;231:462–73.
22. Alitalo K, Tammela T, Petrova TV. Lymphangiogenesis in development and human disease. Nature 2005;438:946–53.
23. Oliver G, Alitalo K. The lymphatic vasculature: recent progress and paradigms. Annu Rev Cell Dev Biol 2005;21:457–83.
24. He Y, Karpanen T, Alitalo K. Role of lymphangiogenic factors in tumor metastasis. Biochim Biophys Acta 2004;1654:3–12.
25. Tobler NE, Detmar M. Tumor and lymph node lymphangiogenesis—impact on cancer metastasis. J Leukoc Biol 2006;80:691–6.
26. Baluk P, Tammela T, Ator E, et al. Pathogenesis of persistent lymphatic vessel hyperplasia in chronic airway inflammation. J Clin Invest 2005;115:247–57.
27. Maruyama K, Ii M, Cursiefen C, et al. Inflammation-induced lymphangiogenesis in the cornea arises from CD11b-positive macrophages. J Clin Invest 2005;115:2363–72.
28. Cursiefen C, Chen L, Borges LP, et al. VEGF-A stimulates lymphangiogenesis and hemangiogenesis in inflammatory neovascularization via macrophage recruitment. J Clin Invest 2004;113:1040–50.
29. Kerjaschki D. The crucial role of macrophages in lymphangiogenesis. J Clin Invest 2005;115:2316–9.
30. Schoppmann SF, Birner P, Stockl J, et al. Tumor-associated macrophages express lymphatic endothelial growth factors and are related to peritumoral lymphangiogenesis. Am J Pathol 2002;161:947–56.
31. Nilsson MB, Langley RR, Fidler IJ. Interleukin-6, secreted by human ovarian carcinoma cells, is a potent proangiogenic cytokine. Cancer Res 2005;65:10794–800.
32. Szlosarek PW, Grimshaw MJ, Kulbe H, et al. Expression and regulation of tumor necrosis factor α in normal and malignant ovarian epithelium. Mol Cancer Ther 2006;5:382–90.
33. Holash J, Davis S, Papadopoulos N, et al. VEGF-Trap: a VEGF blocker with potent antitumor effects. Proc Natl Acad Sci U S A 2002;99:11393–8.
34. Makinen T, Jussila L, Veikkola T, et al. Inhibition of lymphangiogenesis with resulting lymphedema in transgenic mice expressing soluble VEGF receptor-3. Nat Med 2001;7:199–205.
35. Zeisberger SM, Odermatt B, Marty C, Zehnder-Fjallman AH, Ballmer-Hofer K, Schwendener RA. Clodronate-liposome-mediated depletion of tumour-associated macrophages: a new and highly effective antiangiogenic therapy approach. Br J Cancer 2006;95:272–81.
36. Seiler P, Aichele P, Odermatt B, Hengartner H, Zinkernagel RM, Schwendener RA. Crucial role of marginal zone macrophages and marginal zone metallophils in the clearance of lymphocytic choriomeningitis virus infection. Eur J Immunol 1997;27:2626–33.
37. Banerji S, Ni J, Wang SX, et al. LYVE-1, a new

homologue of the CD44 glycoprotein, is a lymph-specific receptor for hyaluronan. J Cell Biol 1999;144:789–801.
38. Cho CH, Koh YJ, Han J, et al. Angiogenic role of LYVE-1-positive macrophages in adipose tissue. Circ Res 2007;100:47–57.
39. Wigle JT, Oliver G. Prox1 function is required for the development of the murine lymphatic system. Cell 1999; 98:769–78.
40. Gerhardt H, Golding M, Fruttiger M, et al. VEGF guides angiogenic sprouting utilizing endothelial tip cell filopodia. J Cell Biol 2003;161:1163–77.
41. Valtola R, Salven P, Heikkilä P, et al. VEGFR-3 and its ligand VEGF-C are associated with angiogenesis in breast cancer. Am J Pathol 1999;154:1381–90.
42. Kubo H, Fujiwara T, Jussila L, et al. Involvement of vascular endothelial growth factor receptor-3 in maintenance of integrity of endothelial cell lining during tumor angiogenesis. Blood 2000;96:546–53.
43. Kaipainen A, Korhonen J, Mustonen T, et al. Expression of the fms-like tyrosine kinase 4 gene becomes restricted to lymphatic endothelium during development. Proc Natl Acad Sci U S A 1995;92: 3566–70.
44. Abernethy NJ, Chin W, Hay JB, Rodela H, Oreopoulos D, Johnston MG. Lymphatic drainage of the peritoneal cavity in sheep. Am J Physiol 1991;260: 353–8.
45. Shibata SJ, Hiramatsu Y, Kaseda M, et al. The time course of lymph drainage from the peritoneal cavity in beagle dogs. J Vet Med Sci 2006;68:1143–7.
46. Hwang SJ, Choi HH, Kim KT, Hong HJ, Koh GY, Lee GM. Expression and purification of recombinant human angiopoietin-2 produced in Chinese hamster ovary cells. Protein Expr Purif 2005;39:175–83.
47. Cao Y. Opinion: emerging mechanisms of tumour lymphangiogenesis and lymphatic metastasis. Nat Rev Cancer 2005;5:735–43.
48. Cueni LN, Detmar M. New insights into the molecular control of the lymphatic vascular system and its role in disease. J Invest Dermatol 2006;126:2167–77.
49. Joukov V, Sorsa T, Kumar V, et al. Proteolytic processing regulates receptor specificity and activity of VEGF-C. EMBO J 1997;16:3898–911.
50. Achen MG, Jeltsch M, Kukk E, et al. Vascular endothelial growth factor D (VEGF-D) is a ligand for the tyrosine kinases VEGF receptor 2 (Flk1) and VEGF receptor 3 (Flt4). Proc Natl Acad Sci U S A 1998;95: 548–53.

Profound but Dysfunctional Lymphangiogenesis via Vascular Endothelial Growth Factor Ligands from CD11b $^{+}$ Macrophages in Advanced Ovarian Cancer

Bong-Hyun Jeon, Cholsoon Jang, Jinah Han, et al.

Cancer Res 2008;68:1100-1109.